



UvA-DARE (Digital Academic Repository)

Materials and devices for spatial multi-dimensional liquid chromatography

Passamonti, M.

Publication date
2022

[Link to publication](#)

Citation for published version (APA):

Passamonti, M. (2022). *Materials and devices for spatial multi-dimensional liquid chromatography*. [Thesis, fully internal, Universiteit van Amsterdam].

General rights

It is not permitted to download or to forward/distribute the text or part of it without the consent of the author(s) and/or copyright holder(s), other than for strictly personal, individual use, unless the work is under an open content license (like Creative Commons).

Disclaimer/Complaints regulations

If you believe that digital publication of certain material infringes any of your rights or (privacy) interests, please let the Library know, stating your reasons. In case of a legitimate complaint, the Library will make the material inaccessible and/or remove it from the website. Please Ask the Library: <https://uba.uva.nl/en/contact>, or a letter to: Library of the University of Amsterdam, Secretariat, P.O. Box 19185, 1000 GD Amsterdam, The Netherlands. You will be contacted as soon as possible.

Chapter 1

General introduction

Abstract

Liquid-chromatography separations are based on a well-established set of principles. The most-important parameters that describe one-dimensional and multi-dimensional liquid chromatography are identified. The potential of spatial multi-dimensional liquid chromatography is explained, resulting in the Separation Technologies for A Million Peaks (STAMP) project. Different kinds of stationary phases are taken into consideration, with the simplicity of *in-situ* creation of monoliths being highlighted. The fundamentals of the polymerization reactions used to create monolithic stationary phases are described. Several materials for 3D-printing column housings and microfluidic devices were explored in this work. Results obtained with glass, polyether ether ketone (PEEK), titanium, and relevant publications on these materials from the last four years are summarized.

1.1 Fundamentals of liquid chromatography

“Tsvetography” was the name given by the legendary botanist Mikhail Tsvet to the technique that he used to separate plant pigments in 1901¹. Today, we would be studying “Tsvetography” if during translation the word *tsvet* (colour in Russian) would not have been translated as *chróma* (colour in Greek), so as to obtain the word chromatography.

Since then, many kinds of chromatographic techniques were developed, but the basic principle remains the same. Chromatography is a process for separating the components of a mixture. The latter is usually introduced in a fluid substance, called the mobile phase, which passes along an immobilized (solid or liquid) stationary phase. Based on different thermodynamic distribution coefficients, the components travel at different (apparent) velocities causing their separation. Various kinetic mechanisms contribute to variations around the average velocity (band broadening).

Liquid chromatography (LC) is one of the most often used chromatographic techniques. Although its resolution power is inferior to that of some of the other chromatographic techniques, such as gas chromatography (GC) or capillary electrophoresis (CE), its applicability is by far the broadest. LC allows the robust and reliable analysis of low- and high-molecular-weight molecules of vastly different polarities (from non-polar to ionic).

In one-dimensional (1D) LC, an analyte moves through a column and its molecules spread out during this process, creating a band. When the latter exits the column, a chromatogram can be recorded, and the band becomes known as a peak. Ideally, each chromatographic band has a Gaussian shape, and its standard deviation (σ) is a measure for the peak width (w). Moreover, each peak is identified by its retention time (t_R) for a given LC system and a given set of conditions. Separation scientists often recur to a better-defined and dimensionless chromatographic property, the retention factor

$$k = \frac{t_R - t_0}{t_0} \tag{1.1}$$

where t_R is the retention time of the analytes and t_0 is the dead time.

The retention factor describes the ratio between the quantity of the analyte in the stationary phase and in the mobile phase and it is directly proportional to the distribution coefficient, K

$$K = \frac{a_s}{a_m} \tag{1.2}$$

where a_s and a_m are the activities of the analyte in the stationary phase and in the mobile phase, respectively. Chromatography is usually performed under conditions of high dilution, where the distribution coefficient in terms of concentrations (K_C) is proportional to K .

In order to describe the separation performance of a chromatographic experiment, other parameters must be taken into account. First, the selectivity (α) is defined as the ratio between the retention factors of two analytes

$$\alpha = \frac{k_2}{k_1} \tag{1.3}$$

where k_2 and k_1 refer to the later and earlier eluting analytes, respectively.

The resolution (R_s) measures the quality of the separation and is defined as the ratio of the distance between two peaks with different retention times and their average widths.

$$R_s = \frac{2(t_{R,2} - t_{R,1})}{w_1 + w_2} \tag{1.4}$$

Chromatographic efficiency is determined by how much the band spreads out in the column before exiting. The peak width is related to the efficiency (N) of the separation, often referred to as the number of (theoretical) plates or plate count

$$N = \left(\frac{t_R}{\sigma_t}\right)^2 = \frac{L}{H} \tag{1.5}$$

Where σ is the standard deviation in time units L is the length of the separation domain and H is the height equivalent of a theoretical plate. The higher the plate height, the lower is the efficiency.

Finally, to develop LC methods, it is convenient to express the resolution, through an approximate equation, as a function of the efficiency, retention factor and selectivity

$$R_s = \frac{\sqrt{N}}{2} \left(\frac{\alpha - 1}{\alpha + 1}\right) \left(\frac{k}{1 + k}\right) \tag{1.6}$$

It is clear from previous equations that the width of the chromatographic band influences the chromatographic efficiency.

In 1956, van Deemter and coworkers² derived an equation in which three factors (A -, B - and C -terms) were introduced that related the column band broadening (plate height) to the interstitial velocity (u).

$$H = A + \frac{B}{u} + C \cdot u \tag{1.7}$$

where A is called the eddy-diffusion term, B is the longitudinal-diffusion term and C is the mass-transfer term. The A -term is related to the multiple paths that an analyte can follow inside the column, due to packing inhomogeneities and small variations of particle size. The B -term depends on the molecular diffusion of the analyte molecules in the longitudinal direction. The C -term is due to the resistance to mass transfer in both the mobile phase and the stationary phase. The linear velocity near the surface of one of the flow-through paths in the column is slower than in the centre of the path, contributing to

broadening the band of the analyte. Analyte molecules will also spend different amounts of time in the stationary phase and in stagnant zones of mobile phase in the pores. When the molecules of the analyte enter the pores, they are held up compared to the molecules that travel in the interstitial space. Different depths of penetration of the analyte molecules cause the band to broaden. Since the derivation of this seminal equation, a number of more-advanced plate-height equations have been proposed. Apart from dispersion within the chromatographic column, there is additional (extra-column) in connection tubing, connectors, injector, and detector.

1.2 Multi-dimensional separation systems

1.2.1 Peak capacity

Nowadays, researchers from many fields such as life science, food science, renewable energy sources, and feedstock need to resolve very complex mixtures in a reasonable time. Chromatograms with many peaks are usually the result of such complex samples. Due to the high abundance of compounds, such chromatograms show peaks that are not fully resolved. In these cases, the resolution (R_s) between two peaks and the efficiency (N) of a column are not the most useful criteria to evaluate the chromatographic performance. Instead, the peak capacity (n) is used to estimate the separation power of a chromatographic system. The peak capacity is defined as the number of peaks that can be separated (with $R_s = 1$) within a retention window.

Two main types of separation approaches can be distinguished – time-based or temporal (t LC) and space-based or spatial (x LC). In the former, the analytes are eluted through a separation domain in time, with the least and the most retained compounds eluting first and last, respectively. In spatial separations, the analytes are separated within the separation domain. The compounds move through the separation bed to a certain position, with the least retained compound moving the furthest.

The peak capacity in 1D- t LC separations is derived from the following differential equation:

$$dn = \frac{dt}{4\sigma_t} \tag{1.8}$$

After integration this yields the following equation for isocratic separations

$$n_{iso} = 1 + \frac{\sqrt{N}}{4R_s} \ln \left(\frac{1 + k_w}{1 + k_a} \right) \tag{1.9}$$

where k_w and k_a are the retention factors of the most- and least-retained compounds, respectively.

For gradient separations, the peak capacity is

$$n_g = \frac{t_g}{4R_s\sigma_t} + 1 \quad (1.10)$$

where t_g is the gradient time.

The peak capacity in 1D- λ LC is derived from the following differential equation:

$$dn = \frac{dx}{4\sigma_x} \quad (1.11)$$

where x is the distance of the spot along the separation domain and σ_x is the standard deviation of the band in length units.

To greatly increase the peak capacity of a separation, whether it is temporal or spatial, it is possible to couple several separation systems so as to create a multi-dimensional LC separation.

1.2.2 Separation performance

Multi-dimensional LC separations have been used mostly in the form of time-based 2D-LC (2D- λ LC). Although it needs improvements, 2D- λ LC has proven to be a successful and fruitful option to resolve complex mixtures. Two main kinds of 2D- λ LC exist *viz.* on-line and off-line. In the off-line approach, fractions of the effluent from the first-dimension (1D) are collected and subsequently transferred and analysed in the second-dimension (2D) separation domain (column). In the on-line approach, the two separation steps follow each other, without interruption. In the comprehensive method (λ LC \times λ LC), the whole effluent of the 1D column is transferred to the 2D column, while in the selective (sLC-LC) or heart-cutting (LC-LC) method, only targeted fractions are analysed in the 2D .

The total analysis time (^{2D}t) and total peak capacity (^{2D}n) of λ LC \times λ LC and space-based 2D-LC (λ LC \times λ LC) can be calculated, according to the following equations

$$^{2D}t = ^1t + ^2t \quad (1.12)$$

$$^{2D}n = ^1n \times ^2n \quad (1.13)$$

When adding a third-dimension (3D), its contribution is added to the equations. The increase in analysis time is noticeable for temporal and spatial separations. However, while in time-based LC only one fraction at the time can be analysed, in spatial separations every spot resulting from the 1D separation can be analysed simultaneously. This notably reduces the total analysis time of λ LC \times λ LC. As far as the peak capacity is concerned, the potential gain is significant for both temporal and spatial LC. However, orthogonality must be taken into account when using Equation (1.1.13). In multi-dimensional chromatography, orthogonality is achieved using different selectivities in the different dimensions of the

separation, so as to cover the whole space of the separation domains. The great potential benefits of spatial multidimensional chromatography have led to significant research efforts in the area^{3,4} and to the development of the Separation Technology for A Million Peaks (STAMP) project. STAMP aims to reach a peak capacity of one million by performing spatial three-dimensional liquid chromatography in 3D-printed microfluidic devices.

1.3 Stationary phases: monoliths and particles

Stationary phases are essential for separating compounds in liquid chromatography. Commercial columns are mostly packed with particles. However, introducing particles in microfluidic devices is not a straightforward process. Confining particles with different selectivities in targeted regions of a microfluidic device can be extremely challenging. Only very limited progress has been made in this direction worldwide, mostly concerning the packing procedure of cylindrical containers (columns)^{5,6} and the associated challenges⁷. In the STAMP project, Roca *et al.*⁸ developed a procedure to uniformly pack a 3D-printed cuboid microfluidic device. The packed device was successfully used to separate a standard mixture of peptides, providing repeatable results.

For these reasons, we mostly focus in this work on monolithic stationary phases. A monolith is a single piece of porous material that can be formed *in-situ* in any housing⁹. Monolithic stationary phases are characterized by macropores and mesopores. The macropores, also known as flow-through pores, typically have an effective diameter of 1 to 2 μm , which allows rapid passage of the mobile phase. Monolithic stationary phases usually exhibit much lower backpressures than packed beds, which is favourable for application in microfluidic devices. The mesopores (typical diameters from 2 to 50 nm) essentially determine the available surface area¹⁰. There are two kinds of monolithic stationary phases, *viz.* those based on silica¹¹ and those based on organic polymers¹². A silica monolith is an inorganic porous material derived from a silane precursor (e.g. tetramethoxysilane). Gelation and the formation of macropores occur within 2 h. After aging and drying mesopores are also formed. These monolithic stationary phases show also micropores (smaller than 2 nm). The time-consuming fabrication process, limited pH range (from 2 to 8), and extensive material shrinkage during synthesis are among the challenges faced when attempting to use silica-based monoliths in LC¹³.

Polymeric monoliths are created by a photochemically or thermally induced polymerization of a mixture consisting of a monomer, a cross-linker, non-reacting solvents ("porogens"), and an initiator. While the monomer provides the functionality, the crosslinker adds rigidity to the final polymer structure. Porogens are often binary mixtures of a "good" and a "bad" solvent, which allows optimization of the conditions to form pores of suitable dimensions. The good porogen, also known as the solvating porogen, is a good solvent for the monomer and the initially formed polymer nuclei. The bad porogen, also known as non-solvating porogen is a poor solvent for both. After the polymerization starts, polymer nuclei are being created. These continue to grow until at some point phase separation starts to occur and a micro-emulsion is formed with two phases, one consisting of the good porogen and the polymers and the other mainly of the bad porogen. Further polymerization and cross-linking cause the polymer to form a porous gel structure that is no longer soluble in the good porogen. The types of porogenic solvents and their

concentrations determine when in the process phase separation occurs (early vs. late phase separation) and the eventual size of the pores and the total pore volume. A high concentration of good porogens results in a late phase separating, the formation of small pores, and a higher surface area. On the other side, a high concentration of bad porogens induces an early phase separation, resulting in the formation of larger pores and a lower surface area^{10,14}. Another factor that affects the ultimate porosity is the concentration of crosslinker. Increasing the concentration of crosslinker in the mixture induces a more-rapid formation of less-soluble polymer and an early phase separation. It also results in smaller globules, smaller pores, and an increase of the surface area¹⁴. Finally, the role of the initiator is to decompose and start the polymerization. The more and the faster the initiator decomposes, the smaller are the globules. The rate of initiation is directly related with the temperature (thermal energy) and/or the radiation energy supplied to the mixture. The higher energy provided to the reaction, the greater the number of radicals formed at the same time. More radicals lead to more, but smaller nuclei and, eventually, smaller pores. Also, the concentration of the initiator is crucial. A higher concentration of initiator in the polymerization mixture also results in smaller pores¹⁵.

Permeability and porosity are main factors that characterize monolithic stationary phases. The simplest method to calculate the permeability (K_f) is by using Darcy's law¹⁶ (Equation 1.1.14):

$$K_f = \frac{F_m \eta L}{\Delta P \pi r^2} \quad (1.14)$$

where F_m is the volumetric flow rate of the solvent, η is its dynamic viscosity, L is the length of the monolith column, ΔP is the pressure drop across it, and r is the radius of the capillary.

The porosity can be characterized using several methods. Scanning electron microscopy (SEM)¹³ is a powerful tool to take "pictures" (micrographs) of monoliths, in order to observe the size of the globules and the pores, as well as the homogeneity of the monolithic bed. Inverse size-exclusion chromatography (I-SEC)¹⁷ uses correlations between the elution times and the molecular size of a small compound and reference polymers to draw conclusions on the porosity and pore-size distribution of the monolithic stationary phases. Another interesting method, referred to as pore blocking, was firstly developed by Cabooter *et al.*¹⁸ and then applied to the monolithic stationary phases by Eeltink *et al.*¹⁹

Porosity is a key feature of monolithic stationary phases from a chromatographic perspective. It is thought that higher linear flow velocities can be used without sacrificing the efficiency of the separation, thanks to the presence of flow-through pores. According to Giddings, resistance to mass-transfer is determined by contributions of dispersion and convection²⁰. In monolithic stationary phases the absence of a stagnant interstitial volume and the presence of flow-through macropores enable an accelerated mass transport, which has been found especially valuable in the gradient-elution separation of high-molecular weight analytes with low diffusion coefficients.

1.4 3D-printing materials: glass, PEEK, titanium

3D-printing, also known as additive manufacturing (AM), is the process of building a three-dimensional object starting from a computer-aided-design (CAD) model. It involves a broad variety of techniques, in

which material is systematically added, typically layer by layer. The main advantages of using 3D-printing include rapid prototyping, fast production of small numbers, cost-effectiveness and fabrication with minimal waste. However, there are also some disadvantages, such as long post-processing, limited choice of materials, and design inaccuracies.^{21,22} The various different techniques of 3D-printing have been introduced in several reviews^{23,24}. Here we will focus only on the three techniques employed in the present work and on the materials used in these processes.

1.4.1 Digital light processing: glass

Digital light processing (DLP) is a 3D-printing technique in which a building tray is partially immersed in a photo-polymerization mixture, contained in a vat. A UV light source and a digital projector are used to project a pre-programmed image on the surface of the object. This causes the monomers to polymerize and cross-links to be formed, creating a new layer on the object. The final object consists of a number of such photopolymer layers. The resolution of this kind of 3D-printer is around 0.15 to 0.2 mm, while the accuracy of the printed part highly depends on the resolution of the projector. In order to improve the resolution, hybrid stereolithography (HSLA) was patented by Nawada²⁵. To achieve a feature size as low as 10 μm , a photomask with a predefined pattern is placed between the photopolymer vat and the projector (digital pattern). Generally, the speed of the DLP 3D-printing process is around 10-20 mm/h, but it has been greatly improved by the introduction of the so-called continuous liquid-interface production (CLIP). The CLIP 3D-printers allow continuous vertical movement of the tray and undisrupted printing at hundreds of mm/h²⁶. Acrylate-based polymers, rigid and flexible polyurethanes, and biocompatible polymers can be 3D-printed using DLP machines. However, all printed polymeric materials have limited organic-solvent compatibility, modest pressure resistance, and low thermal stability. These factors made them unsuitable for application in separation science, such as HPLC.

In 2017, Kotz *et al.*²⁷ 3D-printed objects in transparent silica glass using a stereolithography technique. The procedure consisted of mixing silica nanoparticles in a high concentration (37.5% by volume) with a photocurable resin. The mixture was then used to 3D-print an object, made of silica particles in a polymer matrix (Figure 2a). After a long debinding and sintering process at temperatures up to 1300°C, the object consisted of a non-porous, transparent piece of glass. Glass has a high chemical resistance, and the optical transparency is a great advantage when working with microfluidic devices. Glass objects allow monolithic stationary phases to be formed in confined regions, using a mask for photo-polymerization. Glass also permits to see exactly what happens inside the device. While the preparation of the glass-resin mixture proved simple, 3D-printing parameters were ill-documented. In the present work, we arrived at the parameters reported in Table 1.

Table 1. Parameters used to 3D-print fused-silica transparent glass.

Burn-in layer	300 s
Layer Exposure	200 s
Layer Thickness	100 μm

With the above parameters, we obtained 3D-printed parts with similar resolution as those printed with commercial resins (features of around 0.2 to 0.3 mm). The main problems encountered were related to the “shelf-life” of the resins. Much of the resin solution in the vat is exposed to UV light during the 3D-printing process, causing some polymerization, making the resin solution increasingly viscous over time. While this phenomenon is well-known for all commercial 3D-printing resins, the presence of silica nanoparticles may aggravate the problem. Light scattering, due to differences in refractive index between the resin and the particles, seem to cause a much faster increase in viscosity in glass-containing resin solutions. Consequently, and resolution decreases with time and the repeatability of the process is low, even if fresh resin solution is prepared frequently. After initial post-processing (removal of excess resin solution), the pieces were treated in two ovens for the debinding and sintering steps. Following the work of Kotz²⁷, the debinding step was carried out for 34 h in an ashing furnace, while the sintering step took place in a vacuum tube furnace for almost 14 h. Unfortunately, many of the printed pieces did not survive the debinding process, with cracks and breakages occurring frequently (Figure 2b). Figure 2c shows a device that has been successfully debinded. Warping (deformation) of the device was invariably observed, even when the debinding process was successful. Figure 2d shows some of the most-successful pieces after sintering. The obtained pieces were fragile and unsuitable for HPLC applications. In many cases objects were not transparent (appearing white in Figure 2d). Not a single device could be obtained that was neither broken, nor opaque, nor excessively warped. The low success rate of this time-consuming process made us look for better options.

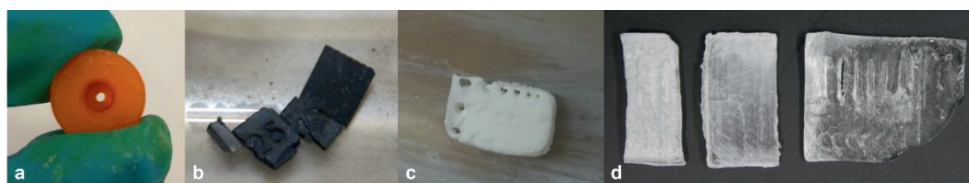


Figure 1. a) 3D-printed piece, b) 3D-printed piece after unsuccessful debinding, c) 3D-printed piece after successful debinding, d) 3D-printed piece after successful sintering.

As of today, the application of the Kotz method²⁷ has been very limited. Other groups developed different methods to 3D-print glass objects. Klein²⁸ used fused-deposition modelling (FDM) to create transparent glass objects, extruding from a heated vessel containing molten glass at about 900°C. Selective laser melting (SLM) was used by Klocke²⁹ and Luo³⁰ to 3D-print a borosilicate and a soda-lime silicate glass, respectively. Finally, Destino *et al.*³¹ prepared a silica glass with high transmittance (> 90%) using a novel 3D-printing technique called direct ink writing (DIW). Although, the promise of 3D-printed glass pieces and their range of possible applications (e.g., microfluidics, optical elements) are enormous, several challenges remain. The high brittleness of the glass, its loss of transparency due to the presence of pores, and the high temperatures involved in its preparation greatly hinder the successful development and proliferation of the methods.

1.4.2 Fused-deposition modelling: PEEK

Conventional FDM printing is based on a filament that is melted and then extruded through a nozzle. The latter is made to move in a programmed manner, according to the CAD design, across a metal plate

("print bed") to deposit material layer by layer. Many polymers such as poly(dimethylsiloxane), poly(lactic acid), acrylonitrile-butadiene-styrene (ABS) polymer, polycarbonate, polystyrene can be 3D-printed using FDM. Unfortunately, many of those polymers show low compatibility with typical LC solvents, such as acetonitrile²¹. Therefore, their chromatographic application is restricted. However, polyether ether ketone (PEEK) is a material often used by separation scientists, due to its outstanding chemical and mechanical properties, retained also at elevated temperatures. PEEK is a thermoplastic polymer with a melting temperature of 343°C, glass transition temperature of 143°C, and operating temperatures up to 260°C³². Moreover, in 2016 Lv *et al.*³³ described a method to covalently anchor a poly(styrene-co-divinylbenzene) monolith to a PEEK surface. This made creating a monolith in a 3D-printed microfluidic PEEK device a viable option that we decided to pursue. Due to its high melting point, the 3D-printing process of PEEK has to be conducted using a modified FDM machine. This 3D-printer has its print bed inside a heated chamber, in order to reduce pore formation and to improve layer interbonding³⁴. We succeeded in 3D-printing the hardware of columns with different internal diameters (from 0.8 to 1.5 mm). Unfortunately, their practical application remained challenging.

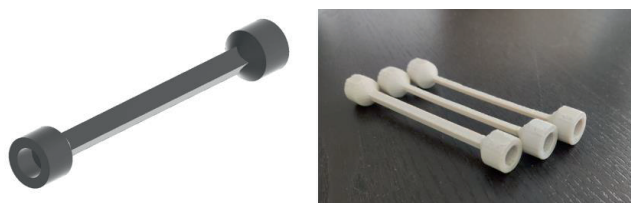


Figure 2. Left) CAD design of a 1.5 mm ID column, right) 3D-printed columns in PEEK with 3 different IDs: 1.5, 1 and 0.8 mm (from closer to further).

3D-printed parts in PEEK have poorer mechanical properties compared to parts produced by conventional manufacturing methods (i.e. injection molding, extrusion). The 3D-printed PEEK pieces showed low elasticity (low Young modulus), making the material very brittle. Also, it has a low tensile strength, which may translate in a limited pressure resistance. Moreover, the fabrication process of monoliths proposed by Lv *et al.*³³ involved a very harsh (concentrated sulphuric acid at elevated temperature) etching process, that caused weakening of the PEEK tubing. Unfortunately, these factors made us desist from pursuing also this path.

1.4.3 Selective laser melting: titanium

SLM is the last 3D-printing method explored and used in this work. SLM is the most-mature 3D-printing technique for metals. A powder bed of small (metal, ceramic, or glass) particles is locally melted and fused by the energy of a laser to create the layers of a 3D-printed object. A broad variety of alloys can be employed, including stainless steel, and alloys of aluminium, tungsten and nickel. For our purpose, a titanium alloy seemed the best choice. Titanium alloy (Ti-6Al-4V) is a strong material that offers excellent mechanical and chemical resistance. Also, after oxidation of the surface, it can be chemically modified using similar reactions as those used to create LC stationary phases. These characteristics make it a good candidate for HPLC applications. This 3D-printed technique has already been applied to created column housings. In 2014, Sandron *et al.*³⁵ 3D-printed a stainless-steel coiled column and

packed it with octadecylsilica particles of different dimensions. The column successfully separated a mixture of uracil and phenones. However, the efficiency of the column was limited due to the roughness of the column wall. In contrast, this wall roughness was used by Gupta *et al.*³⁶ a couple of years later to anchor a poly(butylmethacrylate-co-ethyleneglycoldimethacrylate) monolith to a 3D-printed column in Ti-6Al-4V. The column was further used to separate a mixture of proteins and peptides, achieving a peak capacity of 77. Another use of the SLM printer was the creation of a scaffold in titanium. Vonk *et al.*⁴ created a poly(styrene-co-divinylbenzene) monolith within a 3D-printed scaffold to avoid its rapture. The latter is a common drawback of creating monolithic stationary phases in housings with large internal diameter (> 1 mm). The applications of the SLM 3D-printer in the present work are covered in Chapter 2 and Chapter 4.

1.5 Scope of the thesis

Multi-dimensional separations have great potential for the separation of mixtures with a high degree of complexity. As of today, mostly time-based separations (2D-LC) were successfully used. The demand for resolution power in shorter time frames is what ignited the Separation Technology for A Million Peaks (STAMP) project to explore spatial multi-dimensional LC systems. This thesis aims to *i)* explore 3D-printing materials suitable for the production of microfluidic devices, *ii)* investigate materials to use as stationary phases and their integration in microfluidic devices and *iii)* develop and test 3D-printed microfluidic devices to perform multi-dimensional LC.

Chapter 1 provides a short introduction of the field of study. The principles of LC, time-based and spatial multi-dimensional separation systems are explained. Moreover, it is explained why this work focuses mostly on monolithic stationary phases and their characteristics. Finally, a short overview is provided of the 3D-printing methods and materials explored in this study.

In Chapter 2, the design of two microfluidic devices is described. These were subsequently 3D-printed in a titanium alloy. The aim of these devices was to confine the thermal polymerization of monolithic stationary phases by creating hot and cold regions. The most-successful approach consisted of circulating a liquid at different temperatures through jackets around the channels in the device. The monoliths created in targeted regions of the channels were then characterized and used for the separation of a mixture of proteins.

Chapter 3 describes the optimization of an acrylamide-based polymerization mixture. Monoliths were created in capillaries and characterized in terms of porosity, permeability, and separation performance for a mixture of standard proteins. The best monolithic capillary column was then compared to a packed capillary column using different concentrations of trifluoroacetic (TFA) in the mobile phase. Finally, an attractive hydrophilic-interaction-liquid-chromatography (HILIC) method using a low concentration of TFA on the monolithic column was coupled to mass spectrometry (MS) to evaluate the performance in terms of sensitivity.

Chapter 4 describes a study of the influence of ion-pairing reagents on the separation of intact proteins in HILIC, using silanol-free monolithic stationary phases. The implications of the use of ion-pairing reagents in the sample, in the loading solvent, and in the mobile phases were evaluated in a trap-and-elute set-up. The outcomes of the study were then applied to characterize a complex glycoprotein, *i.e.*, horseradish peroxidase.

In Chapter 5 the design and 3D-printing of microfluidic devices for spatial multi-dimensional separations are described. The devices were evaluated in terms of flow confinement, which led to improvements in the design. Using the results described in Chapter 2, stationary phases were integrated in the devices. Finally, time-based LC separations were achieved.

In Chapter 6 future perspectives and developments in the field of spatial multi-dimensional separations are discussed. The chapter mostly focuses on the technologies and materials that can be used and on possible ways to improve the existing designs.

References

- (1) M.S. Twett. Fiziko-Khimicheskoe Stroenie Khlorofil'nogo Zerna. Eksperimental'noe i Kriticheskoe Izsledovanie.
- (2) van Deemter, J. J.; Klinkenberg, A.; Zuiderweg, F. J. Longitudinal Diffusion and Resistance to Mass Transfer as Causes of Nonideality in Chromatography. *Chem. Eng. Sci.* **1956**, *5* (6), 271–289. [https://doi.org/10.1016/0009-2509\(56\)80003-1](https://doi.org/10.1016/0009-2509(56)80003-1).
- (3) Wouters, B.; Schoenmakers, P. J.; Eeltink, S. Design of a Microfluidic Chip for Spatial Three Dimensional Liquid Chromatography Separations. *18th Int. Conf. Miniaturized Syst. Chem. Life Sci. MicroTAS 2014* **2014**, 2366–2368.
- (4) Vonk, R. J.; Vaast, A.; Eeltink, S.; Schoenmakers, P. J. Titanium-Scaffolded Organic-Monolithic Stationary Phases for Ultra-High-Pressure Liquid Chromatography. *J. Chromatogr. A* **2014**, *1359*, 162–169. <https://doi.org/10.1016/J.CHROMA.2014.07.039>.
- (5) Zelenyánszki, D.; Lambert, N.; Gritti, F.; Felinger, A. The Effect of Column Packing Procedure on Column End Efficiency and on Bed Heterogeneity - Experiments with Flow-Reversal. *J. Chromatogr. A* **2019**, *1603*, 412–416. <https://doi.org/10.1016/J.CHROMA.2019.05.040>.
- (6) Guiochon, G.; Farkas, T.; Guan-Sajonz, H.; Koh, J. H.; Sarker, M.; Stanley, B. J.; Yun, T. Consolidation of Particle Beds and Packing of Chromatographic Columns. *J. Chromatogr. A* **1997**, *762* (1–2), 83–88. [https://doi.org/10.1016/S0021-9673\(96\)00642-5](https://doi.org/10.1016/S0021-9673(96)00642-5).
- (7) Reising, A. E.; Schlabach, S.; Baranau, V.; Stoeckel, D.; Tallarek, U. Analysis of Packing Microstructure and Wall Effects in a Narrow-Bore Ultrahigh Pressure Liquid Chromatography Column Using Focused Ion-Beam Scanning Electron Microscopy. *J. Chromatogr. A* **2017**, *1513*, 172–182. <https://doi.org/10.1016/J.CHROMA.2017.07.049>.
- (8) Liana S. Roca, Theodora Adamopoulou, Suhas H. Nawada, P. J. S. Introduction of Octadecyl-Bonded Porous Particles in 3D-Printed Transparent Housings with Multiple Outlets. *Chromatographia*.
- (9) Svec, F. Porous Polymer Monoliths: Amazingly Wide Variety of Techniques Enabling Their Preparation. *Journal of Chromatography A*. February 5, 2010, pp 902–924. <https://doi.org/10.1016/j.chroma.2009.09.073>.
- (10) Mane, S. Effect of Porogens (Type and Amount) on Polymer Porosity: A Review. *Can. Chem. Trans.* **2016**, *4* (2), 210–225. <https://doi.org/10.13179/canchemtrans.2016.04.02.0304>.
- (11) Nakanishi, K.; Kobayashi, Y.; Amatani, T.; Hirao, K.; Kodaira, T. Spontaneous Formation of Hierarchical Macro-Mesoporous Ethane-Silica Monolith. *Chem. Mater.* **2004**, *16* (19), 3652–3658. <https://doi.org/10.1021/CM049320Y/ASSET/IMAGES/LARGE/CM049320YF00006.JPEG>.
- (12) Nischang, I.; Brueggemann, O.; Svec, F. Advances in the Preparation of Porous Polymer Monoliths in Capillaries and Microfluidic Chips with Focus on Morphological Aspects. *Anal. Bioanal. Chem.* **2010**, *397* (3), 953–960. <https://doi.org/10.1007/s00216-010-3550-x>.
- (13) Švec, F.; Tennikova, T. B.; Deyl, Z. Monolithic Materials: Preparation, Properties and Applications. **2003**, 773.
- (14) Viklund, C.; Svec, F.; Fréchet, J. M. J.; Irgum, K. Monolithic, “Molded”, Porous Materials with High Flow Characteristics for Separations, Catalysis, or Solid-Phase Chemistry: Control of Porous Properties during Polymerization. *Chem. Mater.* **1996**, *8* (3), 744–750. <https://doi.org/10.1021/cm950437j>.
- (15) Xie, S.; Svec, F.; Frechet, J. M. J. Preparation of Porous Hydrophilic Monoliths: Effect of the Polymerization Conditions on the Porous Properties of Poly (Acrylamide-Co-N,N'-Methylenebisacrylamide) Monolithic Rods. *J. Polym. Sci. Part A Polym. Chem.* **1997**, *35* (6), 1013–1021. [https://doi.org/10.1002/\(SICI\)1099-0518\(19970430\)35:6<1013::AID-POLA4>3.0.CO;2-5](https://doi.org/10.1002/(SICI)1099-0518(19970430)35:6<1013::AID-POLA4>3.0.CO;2-5).
- (16) H.Darcy. Les fontaines publiques de la ville de Dijon : exposition et application des principes à suivre et des formules à [...] https://books.google.nl/books/about/Les_fontaines_publicques_de_la_ville_de_D.html?id=42EUAAAQAAJ&redir_esc=y (accessed Jun 19, 2022).
- (17) Urban, J.; Eeltink, S.; Jandera, P.; Schoenmakers, P. J. Characterization of Polymer-Based Monolithic Capillary Columns by Inverse Size-Exclusion Chromatography and Mercury-Intrusion Porosimetry. *J. Chromatogr. A* **2008**, *1182* (2), 161–168. <https://doi.org/10.1016/J.CHROMA.2008.01.006>.
- (18) Cabooter, D.; Lynen, F.; Sandra, P.; Desmet, G. Total Pore Blocking as an Alternative Method for the On-Column Determination of the External Porosity of Packed and Monolithic Reversed-Phase Columns. *J. Chromatogr. A* **2007**, *1157* (1–2), 131–141.

- <https://doi.org/10.1016/J.CHROMA.2007.04.053>.
- (19) Stassen, C.; Desmet, G.; Broeckhoven, K.; Van Lokeren, L.; Eeltink, S. Characterization of Polymer Monolithic Columns for Small-Molecule Separations Using Total-Pore-Blocking Conditions. *J. Chromatogr. A* **2014**, *1325*, 115–120. <https://doi.org/10.1016/J.CHROMA.2013.12.004>.
 - (20) Giddings, J. C. Dynamics of Chromatography: Principles and Theory. *Dyn. Chromatogr. Princ. Theory* **2017**, 1–323. <https://doi.org/10.1201/9781315275871>.
 - (21) Salentijn, G. I.; Oomen, P. E.; Grajewski, M.; Verpoorte, E. Fused Deposition Modeling 3D Printing for (Bio)Analytical Device Fabrication: Procedures, Materials, and Applications. **2017**. <https://doi.org/10.1021/acs.analchem.7b00828>.
 - (22) Ambrosi, A.; Pumera, M. 3D-Printing Technologies for Electrochemical Applications. *Chem. Soc. Rev.* **2016**, *45* (10), 2740–2755. <https://doi.org/10.1039/C5CS00714C>.
 - (23) Gross, B.; Y. Lockwood, S.; M. Spence, D. Recent Advances in Analytical Chemistry by 3D Printing. *Anal. Chem.* **2016**, *89* (1), 57–70. <https://doi.org/10.1021/acs.analchem.6b04344>.
 - (24) Nesterenko, P. N. 3D Printing in Analytical Chemistry: Current State and Future. *Pure Appl. Chem.* **2020**, *92* (8), 1341–1355. <https://doi.org/10.1515/pac-2020-0206>.
 - (25) Nawada, S. H. No Title, 2019.
 - (26) Pagac, M.; Hajnys, J.; Ma, Q. P.; Jancar, L.; Jansa, J.; Stefek, P.; Mesicek, J. A Review of Vat Photopolymerization Technology: Materials, Applications, Challenges, and Future Trends of 3D Printing. *Polym.* **2021**, *Vol. 13*, *Page 598* **2021**, *13* (4), 598. <https://doi.org/10.3390/POLYM13040598>.
 - (27) Kotz, F.; Arnold, K.; Bauer, W.; Schild, D.; Keller, N.; Sachsenheimer, K.; Nargang, T. M.; Richter, C.; Helmer, D.; Rapp, B. E. Three-Dimensional Printing of Transparent Fused Silica Glass. *Nature* **2017**, *544* (7650), 337–339. <https://doi.org/10.1038/NATURE22061>.
 - (28) Klein, J.; Stern, M.; Franchin, G.; Kayser, M.; Inamura, C.; Dave, S.; Weaver, J. C.; Houk, P.; Colombo, P.; Yang, M.; Oxman, N. Additive Manufacturing of Optically Transparent Glass. *3D Print. Addit. Manuf.* **2015**, *2* (3), 92–105. <https://doi.org/10.1089/3DP.2015.0021>.
 - (29) [PDF] Direct Laser Sintering of Borosilicate Glass | Semantic Scholar <https://www.semanticscholar.org/paper/Direct-Laser-Sintering-of-Borosilicate-Glass-Klocke-McClung/87b2041629d79ebb1df84a39c2074c531ded45ed> (accessed May 4, 2022).
 - (30) Luo, J.; Gilbert, L. J.; Qu, C.; Landers, R. G.; Bristow, D. A.; Kinzel, E. C. Additive Manufacturing of Transparent Soda-Lime Glass Using a Filament-Fed Process. *J. Manuf. Sci. Eng. Trans. ASME* **2017**, *139* (6). <https://doi.org/10.1115/1.4035182/366668>.
 - (31) Destino, J. F.; Dudukovic, N. A.; Johnson, M. A.; Johnson, D. T.; Yee, T. D.; Egan, G. C.; Sawvel, A. M.; Steele, W. A.; Baumann, T. F.; Duoss, E. B.; Suratwala, T.; Dylla-Spears, R. 3D Printed Optical Quality Silica and Silica–Titania Glasses from Sol–Gel Feedstocks. *Adv. Mater. Technol.* **2018**, *3* (6), 1700323. <https://doi.org/10.1002/ADMT.201700323>.
 - (32) Zanjanijam, A. R.; Major, I.; Lyons, J. G.; Lafont, U.; Devine, D. M. Polymers Fused Filament Fabrication of PEEK: A Review of Process-Structure-Property Relationships. <https://doi.org/10.3390/polym12081665>.
 - (33) Lv, C.; Heiter, J.; Haljasorg, T.; Leito, I. Covalent Attachment of Polymeric Monolith to Polyether Ether Ketone (PEEK) Tubing. *Anal. Chim. Acta* **2016**, *932*, 114–123. <https://doi.org/10.1016/J.ACA.2016.05.026>.
 - (34) Wu, W. Z.; Geng, P.; Zhao, J.; Zhang, Y.; Rosen, D. W.; Zhang, H. B. Manufacture and Thermal Deformation Analysis of Semicrystalline Polymer Polyether Ether Ketone by 3D Printing. *Mater. Res. Innov.* **2014**, *18* (sup5), S5-12-S5-16. <https://doi.org/10.1179/1432891714Z.000000000898>.
 - (35) Sandron, S.; Heery, B.; Gupta, V.; Collins, D. A.; Nesterenko, E. P.; Nesterenko, P. N.; Talebi, M.; Beirne, S.; Thompson, F.; Wallace, G. G.; Brabazon, D.; Paull, B. 3D Printed Metal Columns for Capillary Liquid Chromatography. *Analyst* **2014**, *139* (24), 6343–6347. <https://doi.org/10.1039/c4an01476f>.
 - (36) Gupta, V.; Talebi, M.; Deverell, J.; Sandron, S.; Nesterenko, P. N.; Heery, B.; Thompson, F.; Beirne, S.; Wallace, G. G.; Paull, B. 3D Printed Titanium Micro-Bore Columns Containing Polymer Monoliths for Reversed-Phase Liquid Chromatography. *Anal. Chim. Acta* **2016**, *910*, 84–94. <https://doi.org/10.1016/J.ACA.2016.01.012>.